Bull Volcanol (2004) 66:671–686
DOI 10.1007/s00445-004-0354-x

RESEARCH ARTICLE

Richard P. Esser · Philip R. Kyle · William C. McIntosh

$^{40}Ar/^{39}Ar$ dating of the eruptive history of Mount Erebus, Antarctica: volcano evolution

Received: 9 November 2001 / Accepted: 29 January 2004 / Published online: 3 June 2004
© Springer-Verlag 2004

Abstract Mt. Erebus, a 3,794-meter-high active polygenetic stratovolcano, is composed of voluminous anorthoclase-phyric tephriphonolite and phonolite lavas overlying unknown volumes of poorly exposed, less differentiated lavas. The older basanite to phonotephrite lavas crop out on Fang Ridge, an eroded remnant of a proto-Erebus volcano and at other isolated locations on the flanks of the Mt. Erebus edifice. Anorthoclase feldspars in the phonolitic lavas are large (~10 cm), abundant (~30–40%) and contain numerous melt inclusions. Although excess argon is known to exist within the melt inclusions, rigorous sample preparation was used to remove the majority of the contaminant. Twenty-five sample sites were dated by the $^{40}Ar/^{39}Ar$ method (using 20 anorthoclase, 5 plagioclase and 9 groundmass concentrates) to examine the eruptive history of the volcano. Cape Barne, the oldest site, is 1,311±16 ka and represents the first of three stages of eruptive activity on the Mt. Erebus edifice. It shows a transition from sub-aqueous to sub-aerial volcanism that may mark the initiation of proto-Erebus eruptive activity. It is inferred that a further ~300 ky of basanitic/phonotephritic volcanism built a low, broad platform shield volcano. Cessation of the shield-building phase is marked by eruptions at Fang Ridge at ~1,000 ka. The termination of proto-Erebus eruptive activity is marked by the stratigraphically highest flow at Fang Ridge (758±20 ka). Younger lavas (~550–250 ka) on a modern-Erebus edifice are characterized by phonotephrites, tephriphonolites and trachytes. Plagioclase-phyric phonotephrite from coastal and flank flows yield ages between 531±38 and 368±18 ka. The initiation of anorthoclase tephriphonolite occurred in the southwest sector of the volcano at and around Turks Head (243±10 ka). A short pulse of effusive activity marked by crustal contamination occurred ~160 ka as indicated by at least two trachytic flows (157±6 and 166±10 ka). Most anorthoclase-phyric lavas, characteristic of Mt. Erebus, are less than 250 ka. All Mt. Erebus flows between about 250 and 90 ka are anorthoclase tephriphonolite in composition.

Keywords Mount Erebus · Geology · Geochronology · $^{40}Ar/^{39}Ar$ dating · Eruptive history · Antarctica · Ross island

Editorial responsibility: J. Donelly-Nolan

R. P. Esser (✉) · P. R. Kyle · W. C. McIntosh
New Mexico Bureau of Geology and Mineral Resources,
New Mexico Institute of Mining and Technology,
801 Leroy Place, Socorro, NM, 87801, USA
e-mail: esser@nmt.edu
Tel.: +1-505-8355217
Fax: +1-505-8356436

P. R. Kyle · W. C. McIntosh
Department of Earth and Environmental Science,
New Mexico Institute of Mining and Technology,
Socorro, NM, 87801-4796, USA

Introduction

Mt. Erebus (77°32′S, 167°10′E), Ross Island, Antarctica is the world's southernmost active volcano. When discovered in 1841 by James Ross, Mt. Erebus was erupting, and it continues to be one of the few volcanoes known to have a persistent, convecting lava lake; it is the only one of phonolitic composition (Kyle et al. 1982; Kyle 1994). Mt. Erebus dominates the landscape on Ross Island, the home to McMurdo Station, center of operations for the National Science Foundation's U.S. Antarctic Program.

The eruptive history of Mt. Erebus is poorly known because snow and ice obscure stratigraphic relationships, and, because prior to this study, only a few conventional K/Ar ages were available. Moore and Kyle (1987) proposed a generalized eruptive history for Mt. Erebus using K/Ar ages from 11 localities (Treves 1968; Armstrong 1978; Moore and Kyle 1987).

Armstrong (1978) dated groundmass and anorthoclase separates from the summit of Mt. Erebus, Fang Ridge and Cape Barne (Fig. 1) and recognized that excess ^{40}Ar ($^{40}Ar_E$) was present in some Erebus samples. He found anomalously old apparent ages for historically erupted anorthoclase and glass. Similar apparent ages for a glass

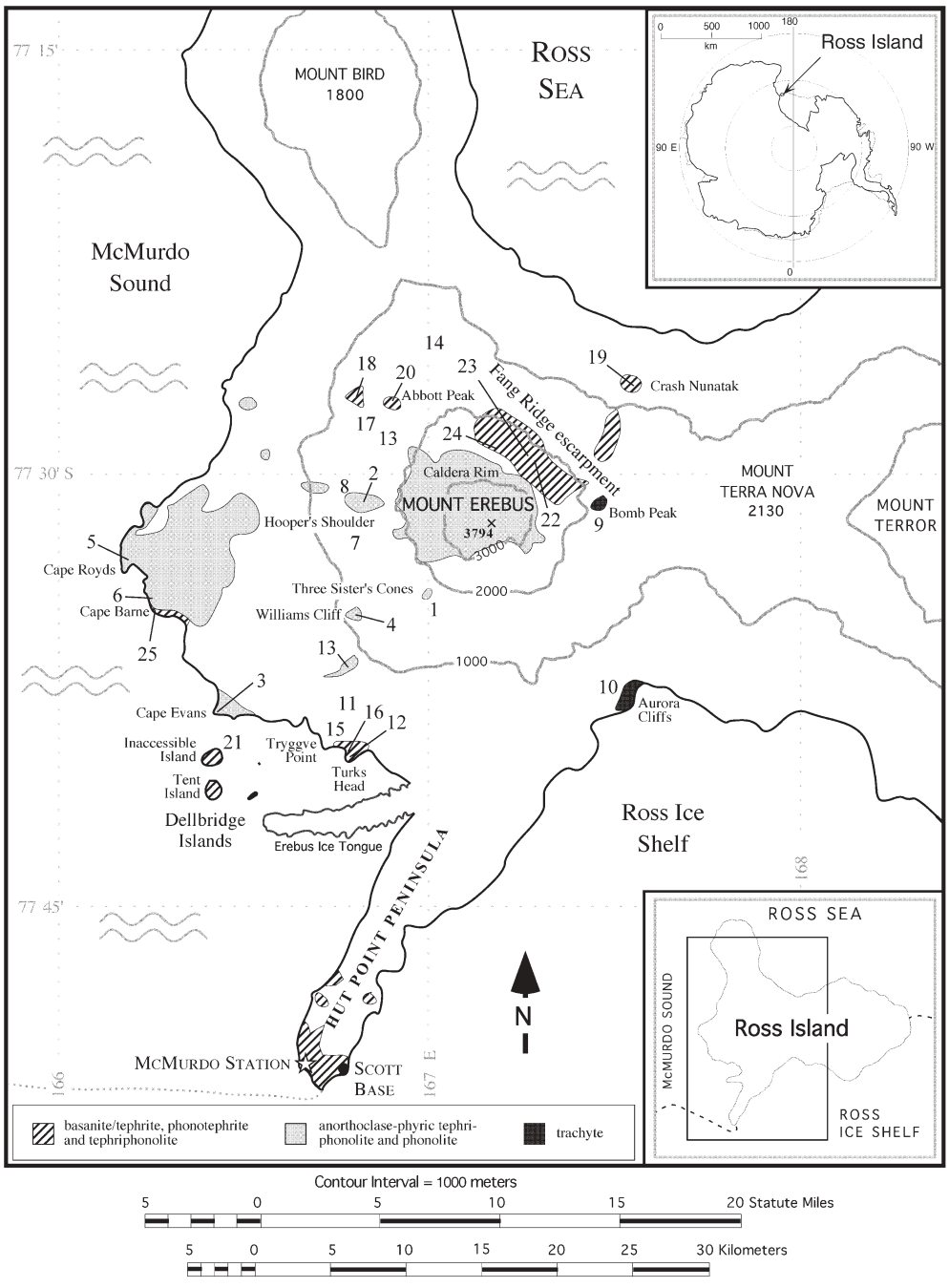

Fig. 1 Generalized geological map of Mt. Erebus and surrounding volcanic centers. *Numbers* on map correspond to sample numbers in Table 1

and associated anorthoclase from an older sample indicated a uniform distribution of excess argon, thereby excluding xenocrysts as the source of the older ages. Because of the probability of $^{40}Ar_E$, Armstrong (1978) recognized that his conventional K/Ar apparent ages were maxima. Esser et al. (1997) showed that much of the $^{40}Ar_E$ is trapped in melt inclusions within the anorthoclase.

The $^{40}Ar/^{39}Ar$ method is capable of revealing and, in many cases, resolving $^{40}Ar_E$ and other complexities that conventional K/Ar dating cannot (Esser et al. 1997). Therefore, this study uses 34 $^{40}Ar/^{39}Ar$ age determinations on 26 samples to yield high-precision apparent ages for 25 sites from Mt. Erebus. Supplemental paleomagnetic data are used to help assess the accuracy of the $^{40}Ar/^{39}Ar$ apparent ages. The combination of the $^{40}Ar/^{39}Ar$ dates and geochemical data contribute to an evolutionary model for the Mt. Erebus volcanic edifice that shows the growth of the volcano over the last million years. The eruptive history of the summit area and age of caldera formation are discussed elsewhere (Harpel et al. 2004).

Volcanic geology of Mount Erebus

Late Cenozoic alkalic volcanic rocks of the McMurdo Volcanic Group (MVG) occur along the western margin of

the Ross Embayment and are informally subdivided into three spatially and tectonically separate volcanic provinces (Hallett, Melbourne, and Erebus volcanic provinces) (Kyle 1990a, 1990b). Magmatism results from intracontinental rifting and extension (Cooper et al. 1987; Kyle 1990a). The Terror Rift, a major graben (Cooper et al. 1987), is bounded to the south by Mt. Erebus and to the north by Mt. Melbourne, another active volcano (Kyle 1990c). Mt. Erebus is surrounded radially at 120° angles by the major eruptive centers Mt. Terror, Mt. Bird and Hut Point Peninsula. Kyle and Cole (1974) suggested that the radial symmetry of the vents resulted from extension during crustal doming. Later, the doming and the extensive volcanism of Ross Island were explained as a result of a hot spot/plume activity (Kyle et al. 1992).

Mt. Erebus is a 3,794-meter-high active polygenetic stratovolcano (Fig. 1). The Mt. Erebus edifice is characterized by multiple stages of eruptive activity resulting in distinctly different morphological features. The lower 1,600 m of the edifice has a low, broad platform shield (slope ≈9°) consistent with low viscosity (mafic?) lavas, although anorthoclase-phyric phonolite lavas comprise most of the exposures. In comparison, the lavas that succeed the shield are more viscous, building at least two steeply sided (>30°) cones. The first cone extends greater than 1,400 m above the top of the platform shield. The remains of this initial cone are manifested by Fang Ridge, a 7-km-long escarpment. The second cone, to the southeast of Fang Ridge, also rises to more than 1,400 m above the top of the platform shield and probably accounts for the entire upper one quarter of the volcanic edifice. The uppermost slopes of the second cone have been modified by a caldera-forming event. The resulting summit caldera (~4 km in diameter) is filled with, and in some cases overflowed by, numerous, small-volume lava flows. Current activity is marked by small strombolian-style eruptions that deposit large bombs on the rim and flanks of the summit cone.

The rocks on Mt. Erebus are composed predominantly of silica-undersaturated basanitic to phonolitic lavas (Kyle et al. 1992). Most of the exposed rocks on Mt. Erebus are anorthoclase-phyric phonolitic lavas. Anorthoclase phenocrysts within lavas are large (up to 10 cm), abundant (~35%) and riddled with melt inclusions (up to 30%) (Kyle 1977; Dunbar et al. 1995). Anorthoclase phonolite and tephriphonolite lava flows are exposed principally on the steep upper slopes. Smaller volumes of anorthoclase phonolite are exposed on the lower flanks, primarily near the coast at Cape Evans, Cape Barne and Cape Royds. The current activity at Mt. Erebus is anorthoclase phonolite in composition.

Unknown volumes of poorly exposed, less chemically differentiated lavas underlie the anorthoclase phonolite flows. Basanitic/tephritic lavas are primarily limited to the platform shield and to the north-northwest sector of the volcanic edifice. Slightly more evolved lavas (phonotephrite to tephriphonolite), some containing large (~2 cm) laths of plagioclase, crop out principally at and around Fang Ridge and other scattered locations on the flanks of the Mt. Erebus edifice (Fig. 1).

The basanitic to phonolitic lava sequence is referred to as the Erebus lineage, and results from the fractional crystallization principally of olivine, clinopyroxene, feldspar, opaque oxides and apatite (Kyle et al. 1992). Basanite/tephrite and phonotephrite commonly contain large phenocrysts (0.5 to 2 cm in length) of plagioclase whereas tephriphonolite and phonolite typically contain large phenocrysts (1 to 10 cm in length) of anorthoclase. Basanite/tephrite is the least evolved lava exposed on Mt. Erebus and is presumed to be the parental melt from which subsequent, younger lavas are derived. Kyle et al. (1992) modeled the fractional crystallization of basanite and suggested phonotephrite, tephriphonolite and phonolite represent 45%, 35% and 23% residual liquids, respectively.

Two small outcrops of trachyte, with <5% anorthoclase phenocrysts, are locally exposed on the slopes of Mt. Erebus. The trachytes are the most differentiated lavas on Mt. Erebus and have higher $^{87}Sr/^{86}Sr$ than the phonolitic rocks, suggesting their evolution involved assimilation as well as fractional crystallization processes (Kyle et al. 1992).

Analytical methods

The twenty-five sites dated in this study were selected to maximize geographic position, compositional range and apparent stratigraphic position. Figure 1 shows the locations of the dated samples as well as prominent geographic place names. Table 1 lists the dated samples, their location names, rock types, laboratory identification and field sample numbers and material separated.

Anorthoclase feldspar was separated from tephriphonolite, phonolite, and trachyte samples, and melt inclusions were removed using methods described by Esser et al. (1997). The resulting anorthoclase was ≥98% pure with a grain size of 150–250 μm. Plagioclase was separated from basanites/tephrites and phonotephrites using similar procedures to those used for the anorthoclase. Because melt inclusions were less abundant in the plagioclase, HF etching times were reduced to 3–6 min. The plagioclase separates had grain sizes of 300–500 μm. In lavas lacking anorthoclase or plagioclase phenocrysts, groundmass concentrates were analyzed. Groundmass concentrates were prepared by removing non-potassium bearing phenocryst phases (e.g. olivine, pyroxene, magnetite). Any carbonates present were removed with 5% nitric acid. Final grain size range of the groundmass concentrates was 300–500 μm.

Samples were irradiated in five batches over a 2-year period. Samples of known weight (40–200 mg) were encapsulated in tin or copper foil and sealed in evacuated quartz vials. The mineral and groundmass sample packets, combined with interspersed Fish Canyon Tuff sanidine (FC-1) monitors, were irradiated in known geometries for 0.5 to 1 h in the L67 position at the University of Michigan's Ford Research reactor under a fast neutron flux of ~7.0×10^{-5} J/h.

All $^{40}Ar/^{39}Ar$ analyses were performed in the New Mexico Geochronology Research Laboratory at the New Mexico Institute of Mining and Technology. J-factor values for the individual irradiations were determined by total fusion of Fish Canyon Tuff sanidine monitors (age=27.84 Ma; Deino and Potts 1990) by resistance furnace or CO_2 laser. Precision for the averaged J-factor results of up to four aliquots per monitor location was typically less than ±0.25% (1σ).

Argon extraction for Mt. Erebus samples was accomplished predominantly using a resistance furnace, but in a few instances, a CO_2 laser was utilized. Laser extraction employed up to two steps of differing wattages followed by reactive gas clean up by a SAES GP-50 getter. Furnace extraction was accomplished by incremental heating in a tantalum or molybdenum crucible using a double-vacuum resistance furnace capable of 1,750 °C. Time at temperature for each heating step was typically 10 min during which reactive gases were removed simultaneously by a SAES AP-10 getter. Further gas cleansing was accomplished in a second stage between the furnace and mass spectrometer using a GP-50 getter. For both extraction techniques, the resulting argon was analyzed using a Mass Analyzer Products (MAP) 215–50 mass spectrometer utilizing an electron multiplier at an approximate gain of 1,000 (sensitivity 2×10^{-17} moles/pA).

Results

Twenty-six samples (12 anorthoclase, 5 plagioclase and 9 groundmass) were dated by the $^{40}Ar/^{39}Ar$ method (Table 1). Three of the samples were dated multiple times to evaluate analytical precision (Table 1). Detailed analytical data can be found at Esser et al. (2003) and online at http://geoinfo.nmt.edu/publications/openfile/argon/home.html. Errors are reported at 2σ, unless otherwise stated. Representative $^{40}Ar/^{39}Ar$ age spectra and analytical data for four samples (two anorthoclase, one plagioclase and one groundmass sample) are presented (Fig. 2, Table 2).

Most anorthoclase age spectra are similar to the sample shown in Fig. 2a (Lab ID #2645). Following a low temperature step with high analytical error, the age spectra remain relatively uniform until about 1,100 °C. At temperatures of 1,200 °C and higher, the apparent age, Cl/K ratio and radiogenic yield increase. The high temperature gas is interpreted to be $^{40}Ar_E$ degassing from melt inclusions within the anorthoclase (Esser et al. 1997), resulting in anomalously old integrated or total gas ages. Because the argon extracted at $\geq$1,200 °C is recognized to contain $^{40}Ar_E$, only the heating steps below 1,200 °C are

Table 1 $^{40}Ar/^{39}Ar$ apparent ages for 25 Mt. Erebus sites

Sample #	Location	Rock type	Lab ID	Field sample #	Latitude (S)	Longitude (E)	Mat.	Method	Age (ka)		Err. (2σ)
1	Three Sister's Cone	A.P.	1329	E80020	77°34′	166°58′	an	plat.	26	±	4
2	Hooper's Shoulder Cone	A.P.	841	E81001	77°32′	166°53′	an	plat.	36	±	8
2	Hooper's Shoulder Cone	A.P.	843	E81001	77°32′	166°53′	an	plat.	28	±	10
2	Hooper's Shoulder Cone	A.P.	1318	E81001	77°32′	166°53′	an	plat.	32	±	10
	Mean age (weighted) n=3								33	±	6
3	Cape Evans	A.T.	427	E83400	77°38′	166°24′	an	plat.	37	±	14
3	Cape Evans	A.T.	1313	E83400	77°38′	166°24′	an	plat.	42	±	8
3	Cape Evans	A.T.	1320	E83400	77°38′	166°24′	an	plat.	32	±	12
3	Cape Evans	A.T.	54	E83400	77°38′	166°24′	an	plat.	53	±	22
	Mean age (weighted) n=4								40	±	6
4	William's Cliff	A.T.	2648	E93020	77°34.81′	166°48.08′	an	plat.	57	±	10
5	Cape Royds	A.T.	1314	E83448	77°32′	166°12′	an	plat.	73	±	10
6	Cape Barne	A.T.	836	E83433	77°35′	166°16′	an	plat.	89	±	4
6	Cape Barne	A.T.	838	E83433	77°35′	166°16′	an	plat.	90	±	12
6	Cape Barne	A.T.	839	E83433	77°35′	166°16′	an	plat.	89	±	4
6	Cape Barne	A.T.	840	E83433	77°35′	166°16′	an	plat.	87	±	8
	Mean age (weighted) n=4								89	±	2
7	SE of Hooper's Shoulder	A.T.	2645	E93021	77°32.35′	166°51.29′	an	plat.	110	±	12
8	NW of Hooper's Shoulder	A.T.	2644	E93011	77°31.023′	166°48.045′	an	plat.	121	±	14
9	Bomb Peak	TR.	1327	E82405	77°30.5′	167°26′	an	plat.	157	±	6
10	Aurora Cliffs	TR.	1321	E83454	77°39.0′	167°28.0′	an	plat.	166	±	10
11	Btwn Williams Cl. and Turks Hd	A.T.	2647	E93019	77°36.660′	166°46.090′	an	plat.	243	±	18
12	Turks Head	A.T.	1315	AW82015	77°40′	166°47′	an	plat.	243	±	10
13	South of Abbott Peak	P.T.	2655	E93024	77°28.632′	166°53.717′	gm	iso.	342	±	18
14	NE of Abbott Peak	P.T.	2653	E93023	77°25.7545	167°01.392′	gm	iso.	364	±	24
15	Tryggve Point dike	P.T.	1536	E77012	77°39′	166°42′	pl	plat.	368	±	18
16	Turks Head	B.	1422	AW82038	77°40′	166°47′	pl	plat.	378	±	28
17	SW of Abbott Peak	PH.	1865	E83453	77°28.3′	166°49.5′	gm	plat.	430	±	40
18	West of Abbott Peak	PH.	2656	E93010	77°27.147′	166°48.841′	gm	iso.	508	±	20
19	Crash Nunatak	PH.	2657	E93008	77°26.678′	167°38.598′	gm	plat.	520	±	120
20	Abbott Peak	P.T.	1326	E81002	77°28′	166°54′	pl	plat.	531	±	38
21	Inaccessible Island	P.	1537	E83407	77°39′	166°21′	gm	plat.	539	±	12
22	Fang Ridge	P.P.	2651	E93005	77°29′	167°12′	pl	iso.	718	±	66
23	Fang Ridge	P.P.	2652	E93007	77°29′	167°12′	pl	iso.	758	±	20
24	Fang Ridge	TE.	2654	E93012	77°29′	167°12′	gm	plat.	1070	±	180
25	Cape Barne dike	B.	1528	E83432	77°34.9′	166 °15.3′	gm	plat.	1310	±	16
25	Cape Barne dike	B.	2658	E93032	77°34.9′	166 °15.3′	gm	plat.	1330	±	60
	Mean age (weighted) n=2								1311	±	16

Rock Type: *A.P.* anorth. phonolite, *A.T.* anorth. tephriphonolite, *P.T.* plag. tephriphonolite, *P.P.* plag. phonotephrite, *PH.* phonotephrite, *P.* phonolite, *TR.* trachyte *TE.* tephrite, *B.* basanite
Mat.: (Material) *an* anorthoclase, *pl* plagioclase, *gm* groundmass
Method: *plat.* plateau, *iso.* isochron
Mean Ages are weighted according to the inverse of the analytical variance for duplicate samples

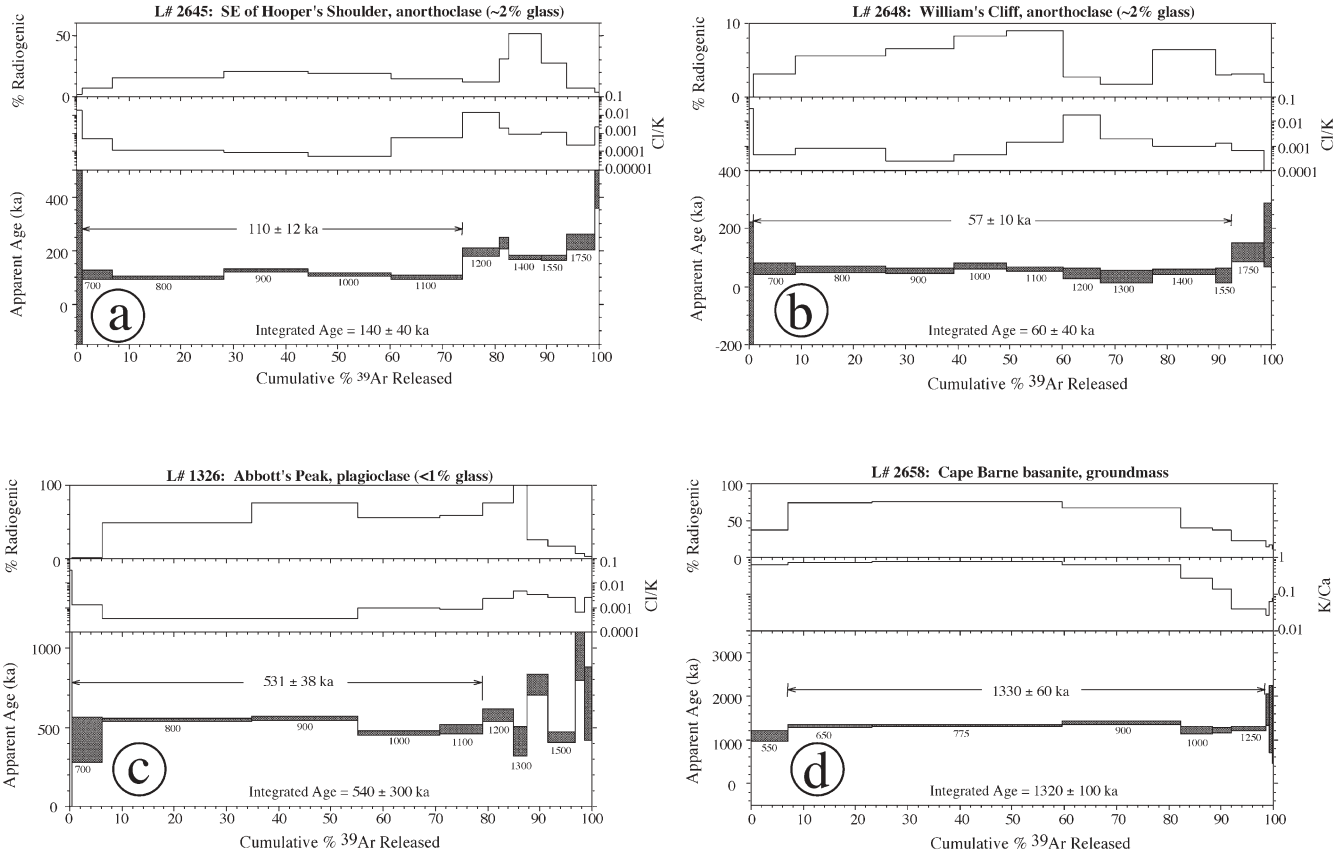

Fig. 2a–d Representative $^{40}Ar/^{39}Ar$ age spectra from Mt. Erebus. **a** and **b** are anorthoclase age spectra from SE of Hooper's Shoulder (sample #7 from Table 1) and William's Cliff (sample #4), respectively. **c** is a plagioclase age spectrum from Abbott's Peak (sample #20) and **d** is a groundmass concentrate age spectrum from a basanite from Cape Barne (sample #25). Errors are given at two-sigma (2σ)

included in a weighted mean age calculation (weighted mean calculated by using the inverse of the variance of each age analysis). The weighted mean or "plateau" occupying the 700 to 1,100 °C steps consistently yields the lowest Cl/K ratios and youngest apparent ages for each sample and usually contains greater than 50% of the cumulative $^{39}Ar_K$ released. Age spectra are calculated using an assumed trapped $^{40}Ar/^{36}Ar$ ratio of 295.5. However, an isotope correlation diagram or inverse isochron ($^{39}Ar/^{40}Ar$ vs. $^{36}Ar/^{40}Ar$) can be used to independently determine the $^{40}Ar/^{36}Ar$ value of the trapped argon. Isotope correlation diagrams plotted for the younger anorthoclase samples are commonly discordant, with MSWD's greater than 10, although apparent ages yielded by 'errorchrons' usually agree with plateau ages at 2σ.

The spectrum for an anorthoclase separate from Williams Cliff (Fig. 2b) differs from other Mt. Erebus anorthoclase samples. Unlike most anorthoclase spectra, it does not show an increase in apparent age with an increase in Cl/K ratio. This suggests that melt inclusions within the Williams Cliff anorthoclase do not contain significant quantities of $^{40}Ar_E$. Similar behavior was noted for anorthoclase samples from a Cape Barne tephriphonolite (e.g. #836). Multiple samples (#836, 838, 839, 840) yielded similar plateau and integrated ages regardless of the quantities of melt inclusions.

Discordant spectra are typical for plagioclase and groundmass samples. This reflects the young ages and low potassium contents in the plagioclase as well as the multiple potassium-bearing phases within the groundmass (Foland et al. 1993; Lo et al. 1994; Singer and Pringle 1996). For most plagioclase and groundmass samples, Cl/K and K/Ca ratios are not correlative with increases in apparent age and do not aid in the interpretation of the age spectra. In most cases, weighted mean ages for plagioclase and groundmass samples were derived from the flattest and youngest portions of the age spectra (Fig. 2).

Inverse isochrons were used for those plagioclase and groundmass samples displaying extreme age spectrum variability. For those samples in which an inverse isochron was used, $^{40}Ar/^{36}Ar$ ratios indicate a trapped component greater than 295.5. The mean square of the weighted deviates (MSWD) for the inverse isochron samples were mostly between 1.0 and 6.0, with the higher values probably reflecting a heterogeneity in trapped argon compositions.

Paleomagnetic data from Funaki (1983) and Mankinen and Cox (1988) and this study were used to help assess the accuracy of seven of the $^{40}Ar/^{39}Ar$ ages (Fig. 3). The

Table 2 $^{40}Ar/^{39}Ar$ analytical data for the anorthoclase, plagioclase and groundmass samples shown in Fig. 2. This data is representative of the majority of samples analyzed in this study

Lab #	Temp (°C)	$^{40}Ar/^{39}Ar$	$^{37}Ar/^{39}Ar$	$^{36}Ar/^{39}Ar$	$^{39}Ar_K$ (moles)	K/Ca	Cl/K	$^{40}Ar^*$ (%)	Cum. ^{39}Ar (%)	Age (ka)		Err (1σ)
E93021:SE of Hooper's Shoulder Cone, 115.5 mg anorth. (~2% glass) J=0.0000755±0.25% Disc.=286.2												
2645-01A	550	2.00e+02	2.84e-01	6.64e-01	3.9e-16	1.8	1.8e-02	1.8	0.87	502	±	1294
2645-01B	700	1.23e+01	5.96e-01	3.89e-02	2.7e-15	0.9	5.6e-04	6.6	6.81	111	±	18
2645-01C	800	4.85e-00	5.72e-01	1.40e-02	9.6e-15	0.9	1.2e-04	15.1	28.15	100	±	6
2645-01D	900	4.52e-00	5.67e-01	1.22e-02	7.2e-15	0.9	10.0e-05	20.6	44.28	127	±	7
2645-01E	1,000	4.31e-00	5.66e-01	1.19e-02	7.1e-15	0.9	5.7e-05	18.9	60.06	111	±	6
2645-01F	1,100	5.07e-00	5.59e-01	1.47e-02	6.2e-15	0.9	6.2e-04	14.7	73.91	102	±	7
2645-01G	1,200	1.15e+01	5.52e-01	3.41e-02	3.1e-15	0.9	1.5e-02	12.4	80.78	194	±	16
2645-01H	1,300	5.44e-00	5.24e-01	1.28e-02	8.6e-16	1.0	2.0e-03	30.8	82.71	228	±	22
2645-01I	1,400	2.48e-00	5.68e-01	4.15e-03	2.8e-15	0.9	9.0e-04	51.5	88.91	174	±	7
2645-01 J	1,550	4.62e-00	5.77e-01	1.14e-02	2.2e-15	0.9	1.1e-03	27.5	93.79	173	±	11
2645-01 K	1,750	2.44e+01	5.62e-01	7.69e-02	2.4e-15	0.9	2.5e-04	6.9	99.21	230	±	29
2645-01L	1,750	1.28e+02	5.53e-01	4.18e-01	3.5e-16	0.9	2.2e-03	3.2	100.00	559	±	202
Total gas age						4.5e-14			*n*=12	140	±	40*
Plateau age							B-F		73.04	110	±	12*
Isochron age				$^{40}Ar/^{36}Ar$=298.4±2.3			MSWD = 20.6			124	±	8*
E93020: William's Cliff, 109.0 mg anorth. (~2% glass) J=0.0000758±0.25% Disc.=286.2												
2648-01A	550	1.88e+02	6.96e-01	6.52e-01	2.3e-16	0.7	3.3e-02	−2.7	0.67	−703	±	926
2648-01B	700	1.48e+01	8.19e-01	4.86e-02	2.8e-15	0.6	4.5e-04	3.1	8.71	63	±	19
2648-01C	800	7.86e-00	8.07e-01	2.53e-02	6.1e-15	0.6	8.2e-04	5.5	26.18	60	±	10
2648-01D	900	6.25e-00	8.30e-01	1.99e-02	4.6e-15	0.6	2.3e-04	6.6	39.27	56	±	10
2648-01E	1,000	6.15e-00	8.37e-01	1.92e-02	3.5e-15	0.6	4.6e-04	8.3	49.32	70	±	11
2648-01F	1,100	4.87e-00	8.30e-01	1.51e-02	3.8e-15	0.6	1.4e-03	9.0	60.19	60	±	9
2648-01G	1,200	1.22e+01	8.11e-01	4.01e-02	2.4e-15	0.6	2.0e-02	2.8	67.14	46	±	19
2648-01H	1,300	1.57e+01	7.87e-01	5.24e-02	3.5e-15	0.6	1.9e-03	1.7	77.28	36	±	21
2648-01I	1,400	5.90e-00	8.36e-01	1.88e-02	4.2e-15	0.6	10.0e-04	6.4	89.25	52	±	9
2648-01 J	1,550	9.18e-00	8.30e-01	3.03e-02	1.0e-15	0.6	1.3e-03	3.0	92.25	38	±	25
2648-01 K	1,750	2.74e+01	8.29e-01	9.00e-02	2.2e-15	0.6	6.8e-04	3.1	98.67	118	±	32
2648-01L	1,750	6.53e+01	8.17e-01	2.17e-01	4.6e-16	0.6	−7.0e-04	2.0	100.00	178	±	111
Total gas age					3.5e-14				*n*=12	60	±	40*
Plateau age							B-J		91.58	57	±	10*
Isochron age				$^{40}Ar/^{36}Ar$ = 293.1±2.9			MSWD = 0.5			65	±	18*
E81002: Abbott Peak tephriphonolite, 107.6 mg plag. (<1% glass) J=0.0000702±0.25% Disc.=288.0												
1326-01A	550	3.67e+03	3.16e-00	1.23e+01	1.6e-17	0.2	3.4e-02	0.6	0.36	2826	±	31565
1326-01B	700	2.03e+02	4.65e-00	6.77e-01	2.5e-16	0.1	1.4e-03	1.6	6.22	420	±	143
1326-01C	800	8.91e-00	5.04e-00	1.68e-02	1.2e-15	0.1	3.9e-04	48.3	34.77	546	±	8
1326-01D	900	5.84e-00	5.26e-00	6.23e-03	8.7e-16	0.1	3.7e-04	75.0	55.13	556	±	10
1326-01E	1,000	6.52e-00	4.42e-00	1.08e-02	6.7e-16	0.1	9.7e-04	55.9	70.85	463	±	13
1326-01F	1,100	6.52e-00	4.77e-00	1.03e-02	3.6e-16	0.1	9.0e-04	58.7	79.12	486	±	30
1326-01G	1,200	5.98e-00	4.00e-00	5.80e-03	2.5e-16	0.1	2.4e-03	76.1	84.86	578	±	38
1326-01H	1,300	2.93e-00	3.52e-00	−2.47e-04	1.1e-16	0.1	4.6e-03	111.0	87.52	412	±	93
1326-01I	1,400	2.35e+01	4.54e-00	6.01e-02	1.7e-16	0.1	3.4e-03	25.7	91.50	767	±	67
1326-01 J	1,500	1.93e+01	3.96e-00	5.47e-02	2.3e-16	0.1	2.6e-03	17.8	96.88	437	±	34
1326-01 K	1,550	1.25e+02	5.39e-00	3.98e-01	7.1e-17	0.1	7.2e-04	6.6	98.53	1044	±	251
1326-01L	1550	1.46e+02	3.90e-00	4.79e-01	6.3e-17	0.1	2.6e-03	3.5	100.00	647	±	232
Total gas age					4.3e-15				*n*=12	540	±	300*
Plateau age							B-F		78.76	531	±	38*
Isochron age				$^{40}Ar/^{36}Ar$=295.0±4.1			MSWD = 15.3			536	±	14*

Table 2 (continued)

Lab #	Temp (°C)	$^{40}Ar/^{39}Ar$	$^{37}Ar/^{39}Ar$	$^{36}Ar/^{39}Ar$	$^{39}Ar_K$ (moles)	K/Ca	Cl/K	$^{40}Ar^*$ (%)	Cum. ^{39}Ar (%)	Age (ka)		Err (1σ)
E93032: Cape Barne basanite 103.7 mg groundmass J=0.0000759±0.25% Disc.=286.2												
2658-01A	550	2.16e+01	7.91e-01	4.61e-02	2.3e-15	0.6	8.4e-02	37.0	7.02	1096	±	119
2658-01B	650	1.31e+01	7.11e-01	1.18e-02	5.2e-15	0.7	6.4e-02	73.7	22.64	1322	±	41
2658-01C	775	1.28e+01	6.43e-01	1.03e-02	1.2e-14	0.8	7.6e-02	76.3	59.24	1338	±	22
2658-01D	900	1.53e+01	8.19e-01	1.75e-02	7.6e-15	0.6	6.4e-02	66.6	82.04	1401	±	33
2658-01E	1,000	2.20e+01	1.85e-00	4.48e-02	2.0e-15	0.3	5.4e-02	40.4	88.09	1219	±	79
2658-01F	1,100	2.38e+01	3.77e-00	5.13e-02	1.2e-15	0.1	4.0e-02	37.5	91.72	1227	±	60
2658-01G	1,250	4.08e+01	1.28e+01	1.11e-01	2.3e-15	0.0	1.3e-01	22.2	98.61	1253	±	48
2658-01H	1,400	8.20e+01	1.85e+01	2.41e-01	2.1e-16	0.0	1.4e-01	14.8	99.23	1685	±	363
2658-01I	1,750	6.38e+01	8.24e-00	1.81e-01	1.8e-16	0.1	2.6e-02	16.9	99.76	1483	±	771
2658-01 J	1,750	5.51e+01	6.64e-00	1.66e-01	7.9e-17	0.1	1.6e-03	11.9	100.00	903	±	437
Total gas age					3.3e-14				*n*=10	1320	±	100*
Plateau age							A-G		98.61	1330	±	60*
Isochron age				$^{40}Ar/^{36}Ar$= 288.9±3.3			MSWD = 2.3			1355	±	36*

Isotopic ratios corrected for blank, radioactive decay, and mass discrimination, not corrected for interfering reactions
Individual analyses show analytical error only; plateau and total gas age errors include error in J and irradiation parameters
Flux Monitor (Fish Canyon sanidine)=27.84 Ma
Disc.=Mass Discrimination (1 a.m.u.)
Correction Factors: $(^{40}Ar/^{39}Ar)_K$=0.022; $(^{36}Ar/^{37}Ar)_{Ca}$=0.00026; and $(^{39}Ar/^{37}Ar)_{Ca}$=0.00070
K/Ca=0.510×$(^{39}Ar_K/^{37}Ar_{Ca})$; Cl/K=0.277×$(^{39}Ar_K/^{38}Ar_{Cl})$
All samples in Table 2 were analyzed using the resistance furnace (heating time=10 min; reactive gas clean-up time=5 to 8 min)
Spectrometer sensitivity=2.0×10^{-17}moles/pA
Total system blanks were between $7\times10^{-16}$and 3×10^{-15}moles ^{40}Ar
Plateau (weighted mean) age calculated by weighting each age analysis by the inverse of the variance
Plateau (weighted mean) error calculated using the method of Taylor (1982)
Plateau ages are weighted by the inverse of the variance whereas total gas ages are weighted by ^{39}Ar
Errors marked with an asterisk (*) are given at 2σ all others are given at 1σ
Errors include the uncertainty in J-values (±0.25%)
Ages are calculated using the decay constants recommended by Steiger and Jäger (1977)

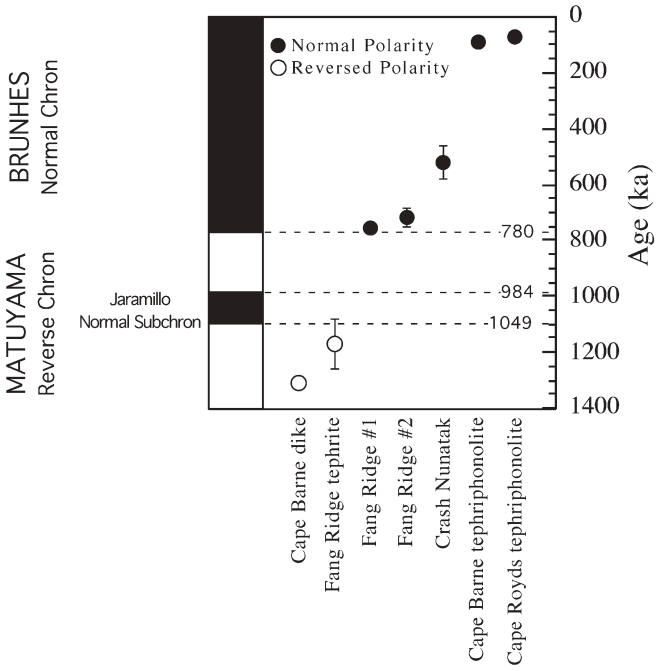

Fig. 3 $^{40}Ar/^{39}Ar$ apparent age/paleomagnetic correlations for Mt. Erebus lava flows where magnetic directions are known. Cape Royds paleomagnetic samples are from Funaki (1983) while Cape Barne tephriphonolite and dike are from Mankinen and Cox (1988). All other data are from this study. Errors on ages are two sigma and in some cases are smaller than the symbol

Cape Barne dike and the Fang Ridge tephrite have reversed polarity and the $^{40}Ar/^{39}Ar$ ages for these two samples fall within the Pre-Jaramillo segment of the Matuyama reverse polarity interval (1,757–1,049 ka; Cande and Kent 1992). Two additional Fang Ridge samples (normal polarity) fall near the beginning of the Brunhes normal polarity event (780–0 ka; Cande and Kent 1992). The remaining three samples are significantly less than 700 ka and have normal polarity.

Discussion

$^{40}Ar/^{39}Ar$ measured ages for Mt. Erebus samples are up to one order of magnitude younger and more precise than the previously determined K/Ar ages. For example, $^{40}Ar/^{39}Ar$ ages of 89±2 and 73±10 ka for lavas at Cape Barne and Cape Royds, respectively, compare to K/Ar ages of 965±100 and 698±280 ka (2σ; Treves 1968; Armstrong 1978). The differences between K/Ar ages and $^{40}Ar/^{39}Ar$ ages can largely be explained by the effect of $^{40}Ar_E$ in melt inclusions (Esser et al. 1997).

There is evidence that melt inclusions in some anorthoclase contain little or no $^{40}Ar_E$. $^{40}Ar/^{39}Ar$ apparent plateau ages for four anorthoclase (two glass-rich and two 'pure') samples from Cape Barne are identical at 1σ regardless of their individual Cl/K ratios. By comparison, a $^{40}Ar/^{39}Ar$ plateau age for 'pure' anorthoclase from the upper flank outcrop of Hooper's Shoulder was 32±12 ka, whereas the mean age for the glass-rich Hooper's Shoulder anorthoclase over the same argon-extraction temperature interval was 84±24 ka.

It is important to stress that all of the $^{40}Ar/^{39}Ar$ apparent ages from Mt. Erebus should be considered maxima. Based on the $^{40}Ar/^{39}Ar$ apparent ages of historically erupted (i.e. zero-age) anorthoclase phenocrysts (20±3 ka) (Esser et al. 1997), a general geological "uncertainty" may be incorporated into the apparent age of the non-zero-age samples from Mt. Erebus. Assuming the non-zero-age anorthoclase samples are as pure as the purest zero-age anorthoclase samples, a maximum of 20,000 years of excess argon may have been contributed to the apparent ages of all anorthoclase samples. However, this large geological uncertainty is probably not appropriate for all of the dated anorthoclase samples as many yield little or no evidence of excess argon (e.g. Cape Barne and William's Cliff). Regardless, the $^{40}Ar/^{39}Ar$ apparent ages of this study represent a significant increase in the overall precision of dating young anorthoclase from Mt. Erebus and therefore allow development of a more comprehensive volcanic evolutionary model.

Volcanic evolution

Three stages of eruptive activity are inferred from the $^{40}Ar/^{39}Ar$ apparent ages (Fig. 4) and are discussed below.

>1,311–1,000 ka: shield building phase

Initial eruptive activity at Ross Island and Mt. Erebus probably involved the extrusion of basanitic pillow lavas and associated submarine pyroclastic rocks onto the floor of the Ross Sea. These earliest eruptive products have been buried by subsequent activity. The current Ross Sea depth is greater than 700 m less than 10 km off shore (1:250,000 USGS Map of Ross Island). Although water depths have presumably been affected by sea level fluctuations and isostatic subsidence, the initial eruptive environment at Ross Island was certainly submarine. Unequivocal evidence for subaqueously erupted Ross Island volcanic rocks was recovered by the Dry Valley Drilling Project (DVDP) cores 1, 2 and 3 at Hut Point Peninsula (Kyle 1981a). K-Ar dates on drill core basanitic hyaloclastites (1,340±230 ka) (Kyle 1981a) are contemporaneous with the earliest dated activity at Mt. Erebus in this study.

The oldest dated volcanic rock (1,311±16 ka) on Mt. Erebus is from a highly fractured and weathered tephritic dike intruding one of three cones of pyroclastic beds, lavas and palagonitized hyaloclastite tuff at Cape Barne. The dike was probably a feeder to the cone which has characteristics of both subaerial and subaqueous volcanic activity (Moore and Kyle 1987). This exposure marks a transition from subaqueous to subaerial activity at this location at 1,300 ka.

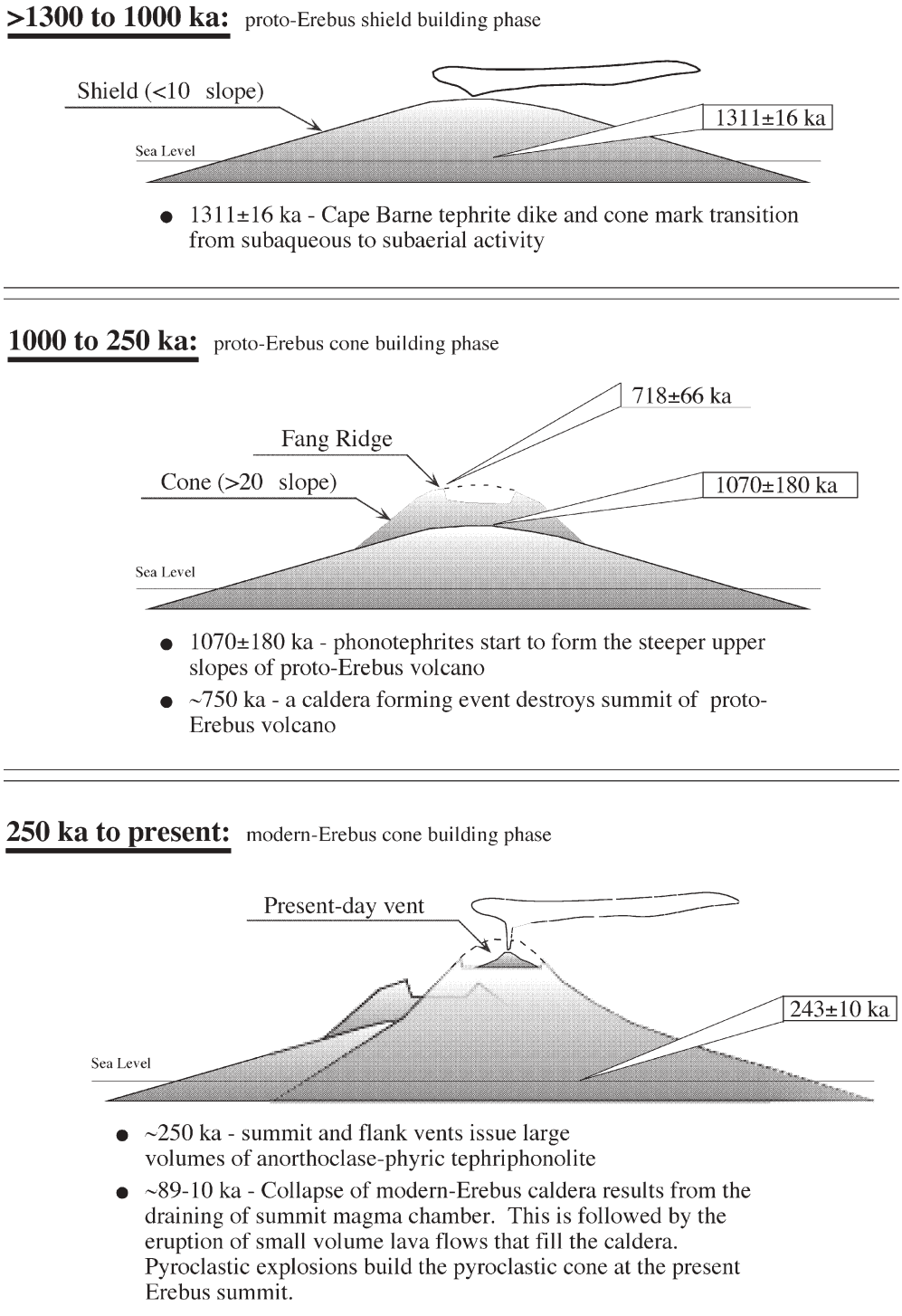

Fig. 4 Schematic representation of evolution of Mt. Erebus from greater than 1,300 ka to present

Following the emplacement of the Cape Barne cones and associated dike at 1,311±16 ka, subaerial vents probably continued to erupt undifferentiated basanitic/tephritic lava. These relatively low viscosity lavas likely formed the broad shield-like platform (slope ≈9°) visible today at elevations between 0 and 1,600 m a.s.l. The basanite/tephrite shield reached a final elevation of at least 2,600 m a.s.l. approximately 1 million years ago, as revealed by the current elevation of a 1,070±180 ka basanite/tephrite flow at Fang Ridge that is inferred to be one of the last flows of this composition on Mt. Erebus. Presumably, any lava flows between 1,300 and 1,000 ka are buried by subsequent, younger lava flows and snow and ice, as no rocks in this age range have been identified on Mt. Erebus.

~1,000–250 ka: proto-Erebus cone building phase

Between approximately 1,250 and 890 ka, the basanitic/tephritic activity on Mt. Erebus gave way to eruptions of

more differentiated lavas including phonotephrite and tephriphonolite. The more viscous phonotephrite and tephriphonolite lavas were erupted on top of the older, less differentiated lavas and are responsible for the steeper upper slopes of proto-Erebus, which are currently preserved at Fang Ridge. Slopes in excess of 35° above elevations of 2,000 m contrast sharply to the shallow 9° slopes of the lower shield. Although stratigraphic and $^{40}Ar/^{39}Ar$ age relationships verify the basanitic to phonotephritic/tephriphonolitic transition at Fang Ridge (Moore and Kyle 1987), large uncertainties in the apparent ages for those samples hamper the formulation of a detailed geologic history. The $^{40}Ar/^{39}Ar$ results indicate the elapsed time between eruptions of the stratigraphically lowest lava flow (1,070±180 ka) and stratigraphically highest lava flow (718±66 ka) at Fang Ridge could have been between 106 and 598 ky, assuming 2σ error ranges. The relatively large time span (approximately one-third of the total assumed age of proto-Erebus) coincides with the emplacement of less than 200 m of vertically stacked flows at Fang Ridge. This suggests an eruption rate for Fang Ridge that is significantly less than what is deduced for earlier, and observed for later, proto-Erebus and modern-Erebus activity, respectively. Alternatively, the halt in tephrite activity could mark a period of repose, whereby magma chamber differentiation produced the phonotephrites and tephriphonolites.

Following the eruption of the youngest Fang Ridge tephriphonolites at 758±20 and 718±66 ka, a catastrophic event created a large escarpment from the upper flank area of proto-Erebus. Today, this escarpment is manifested by Fang Ridge, a prominent NW–SE-striking ridge with a steep (>35°), northeast-facing slope and a vertical, southwest-facing cliff greater than 150 m tall. Fang Ridge is a roughly linear feature at least 7 km in length, situated 2,000 to 3,000 m a.s.l and at least 1,000 m northeast of the steep upper slopes of the anorthoclase phonolite section of Mt. Erebus (Fig. 1). Although the middle of Fang Ridge achieves a topographic high of greater than 3,000 m, the southeast and northwest ends of the scarp are about 200 and 400 m lower in elevation, respectively. These topographically lower margins, especially in the northwest sector, may indicate that the summit crater was breached either contemporaneous with or subsequent to crater formation. Fang Ridge is somewhat concave toward the southwest, though later anorthoclase phonolite flows obscure the true outline of the proto-Erebus feature. Although a large proportion of the proto-Erebus crater is buried beneath snow and ice, and later anorthoclase phonolite flows, extrapolation of the existing scarp at Fang Ridge suggests a depression approximately 5 km in diameter (Fig. 5). The center of this depression may approximate the location of the proto-Erebus vent, about 2 km north of the current modern-Erebus vent.

The two most probable scenarios to account for the large escarpment at Fang Ridge are sector collapse or subsidence. However, evidence of either is incomplete. Volcanic sector collapse occurs when interdigitating unconsolidated pyroclastic material and lava result in the gravitational instability of a slope (Siebert 1984). The steep upper slopes and pyroclastic material of proto-Erebus would be sufficient to generate sector collapse. A mass movement occurrence may have been directed to the southwest, leaving Fang Ridge relatively intact (Fig. 5). Although a large volume of anorthoclase phonolite (modern-Mt. Erebus) lies directly southwest of Fang Ridge, no identifiable remains of the collapse feature are found down slope of what would have been the proto-Erebus summit. While it is possible that the younger anorthoclase phonolite flows (e.g. Hooper's Shoulder, Three Sister's Cones, William's Cliff, etc.) conceal the majority of the flank deposits, the long run-out distances typical of volcanic collapse features (Siebert 1984) may mean that any collapse deposits are concealed beneath McMurdo Sound. To date, no deposits resembling collapse breccia have been identified anywhere on Mt. Erebus.

Subsidence, rather than sector collapse, may have created Fang Ridge and an associated caldera. Caldera subsidence occurs when (1) large quantities of magma evacuate a magma chamber or dike system leaving the overlying crust unsupported (Macdonald 1965), or (2) when shallow intrusions cause crustal loading (Walker 1988). Both mechanisms result in the collapse of the overlying roof material. However, physical evidence of either mechanism is, again, incomplete. Although volcanoes comparable in composition to Mt. Erebus are known to erupt explosively and non-explosively (Chester et al. 1985; Guest et al. 1988; Ancochea et al. 1990; van den Bogaard 1995), the absence of large quantities of primary pyroclastic material at Mt. Erebus likely constrains subsidence to either 'passive' magma withdrawal or crustal loading. Passive magma withdrawal is usually characterized by eruptions at non-summit vents (Macdonald 1965). No lateral or parasitic vents from the presumed time of collapse (~700 ka) have been identified on Mt. Erebus. However, concealment by snow, ice, erosion and/or younger flows may make recognition impossible. Similarly, subsidence due to shallow dike and sill loading cannot be confirmed due to the undissected nature of the volcano. Lack of evidence to distinguish among the three escarpment-forming scenarios (collapse, magma withdrawal, or crustal loading) prevents a definitive interpretation. Unequivocal evidence for caldera subsidence at the modern-Erebus summit $\leq$75 ka (Harpel et al. 2004) suggests a similar event may have occurred on proto-Erebus about 700 ka.

The precise timing of the Fang Ridge crater is not known. The maximum age of its formation is constrained by the stratigraphically highest Fang Ridge flow at 718±66 ka. No proto-Erebus lava flows younger than 700 ka have been identified within the Fang Ridge crater, making an estimate of the minimum age of formation speculative. Likewise, no lava flows between about 700 and 540 ka have been identified on the proto-Erebus flanks. Lava flows dated at approximately 540–500 ka are exposed on the flanks of proto-Erebus, but their relationship to the proto-Erebus crater is not known. The

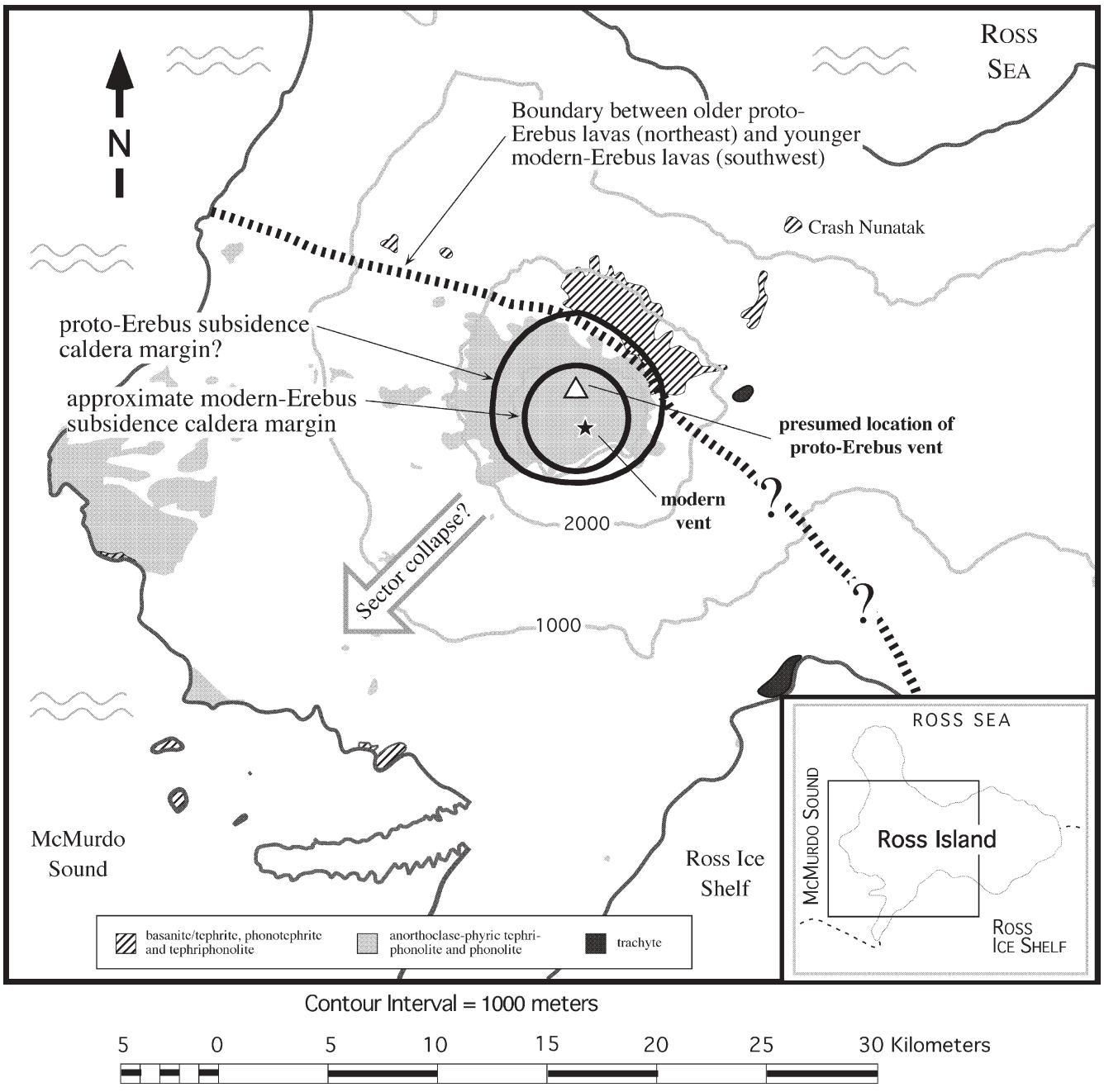

Fig. 5 Topographic map of Mt. Erebus showing approximate locations of proto-Erebus (*large arrow* shows direction of mass movement necessary for sector collapse scenario) and modern-Erebus craters/calderas. *Dotted margin* separates older, more mafic lavas from the young, anorthoclase-phyric lavas

apparent 150–200-ky period of relative inactivity following the formation of the Fang Ridge escarpment may have resulted in chemically more evolved tephriphonolite magma erupted near Abbott Peak, Crash Nunatak and surrounding areas from 531±38 to 508±20 ka.

Flank activity, more characteristic of proto-Erebus, continued after an eruptive lull between 500 and 400 ka, with the eruption and emplacement of lavas primarily southwest (430±40 ka), northeast (364±24 ka) and south of Abbott Peak (342±18 ka). The vents for these flows are unknown. The phonotephritic compositions of the flows, as represented by the sample southwest of Abbott Peak, are less differentiated than older tephriphonolitic flows at Abbott Peak (i.e. 531±38 ka). This may suggest the injection of significant quantities of new, undifferentiated basanitic(?) melt into the proto-Erebus plumbing system.

Flank vents are found near the southwestern coast of Ross Island, at the Dellbridge Islands (Fig. 1). The islands consist of sequences of pillow lavas, pyroclastic breccias and individual flows dipping 2–40° in directions that are

not perpendicular to the axis of flow from the summit of Mt. Erebus. The islands are interpreted to be remnants of cones formed early in the activity at Mt. Erebus (Moore and Kyle 1987). A $^{40}Ar/^{39}Ar$ date on a phonolite lava from one of the Dellbridge Islands, Inaccessible Island (539±12 ka), and the seemingly accelerated petrologic evolution of the stratigraphically oldest to youngest flows (Moore and Kyle 1987) compared to the rest of the Erebus edifice suggest that the Dellbridge Islands were active for a comparatively short period of time and were erupted from a magma chamber separate from that of the Mt. Erebus edifice. The Inaccessible Island phonolite is geochemically more differentiated and mineralogically distinct from contemporaneous proto-Erebus lavas and is stratigraphically overlain by less evolved tephriphonolite (Moore and Kyle 1987). Younger tephriphonolite sequences displaying subaqueous and subaerial activity similar to that at Inaccessible Island have been identified at Turks Head and Tryggve Point, 5 km east of the Dellbridge Islands (Moore and Kyle 1987). Based on the similarities between the Turks Head/Tryggve Point succession and the Dellbridge Island succession, Kyle (1976) and Moore and Kyle (1987) interpreted the two locations to be parts of the same eruptive center on the lower flanks of the volcano. Two $^{40}Ar/^{39}Ar$ dates from tephriphonolites at Turks Head (378±28 ka) and Tryggve Point (368±18 ka) suggest that the Dellbridge Islands center may have been active for over 150 ky.

~250 ka–present: modern-Erebus cone building phase

The first anorthoclase-phyric eruptions begin at approximately 250 ka, marking the transition from proto-Erebus to modern-Erebus activity. Following the cessation of the activity at the Dellbridge Islands center, a younger flow (243±10 ka) of slightly more evolved anorthoclase-phyric tephriphonolitic composition was emplaced over the ca. 375-ka plagioclase-phyric lava flows at Turks Head (Moore and Kyle 1987). Although the 243 ka flow is geochemically similar to the stratigraphically highest flows at Inaccessible and Tent Island (Moore 1986), its source is probably higher up on the slopes (summit?) of the Erebus edifice as suggested by a flow of analytically indistinguishable age (243±18 ka) and similar composition found at Williams Cliff 850 m above Turks Head. These tephriphonolites may indicate the approximate time when eruptive activity shifted from proto-Erebus flank vents to summit vents, marking the cone-building phase of modern-Erebus. The anorthoclase tephriphonolite summit vent is currently at least 2 km south-southwest of the presumed proto-Erebus summit vent, based on the morphology of the Fang Ridge escarpment.

Following the eruption and emplacement of the ca. 230-ka tephriphonolite(s) at and above Turks Head, sporadic trachytic activity occurred on the upper and lower flanks of the Erebus edifice (west and southwest sector). Bomb Peak (157±6 ka) is a small (100 m high) endogenous trachyte dome approximately 5 km east and 1,500 m below the currently active Mt. Erebus summit. Aurora Cliffs (166±10 ka) is a sequence of subglacial to subaerial trachyte on the present shore of Ross Island approximately 15 km south of Bomb Peak (Moore 1986). Both Bomb Peak and Aurora Cliffs trachyte are geochemically suggestive of contamination by crustal material (Kyle et al. 1992) and therefore are not representative of the evolution of the Erebus lineage lavas. Given the similarity in $^{40}Ar/^{39}Ar$ apparent ages and chemical composition between the Bomb Peak and Aurora Cliffs trachytes to the Turks Head tephriphonolites (ca. 250 ka), it is conceivable that the trachytes evolved by assimilation and fractional crystallization (AFC) of the tephriphonolites (Kyle et al. 1992).

The time interval between 250 ka and about 90 ka marks a significant increase in Mt. Erebus activity, likely representing the bulk of the volcanic edifice. After the eruption of the trachytes at Bomb Peak and Aurora Cliffs, large volumes of anorthoclase-phyric tephriphonolite continued to issue from vents located at the Mt. Erebus summit and upper flanks. Tephriphonolite sampled from exposures between 1,600–1,800 m a.s.l. on the western flanks of the volcano yield $^{40}Ar/^{39}Ar$ ages of 121±14 and 110±12 ka. Although these flows may have erupted from a proposed lateral or flank vent near Hooper's Shoulder (Moore and Kyle 1987), the majority of lava flows during this time period (120–90 ka) likely originated from the summit. This is supported by a large quantity of long (up to 5 km) and large (up to 50 m wide) flows and flow levees of tephriphonolitic composition exposed on the steep upper slopes of Mt. Erebus. The radiating pattern of these flows suggests that their source area was a central summit vent. The upper ends of these steep lava flows are truncated by an escarpment containing a flow with a $^{40}Ar/^{39}Ar$ age of 87±14 ka (Harpel et al. 2004). The 87±14 ka exposure may mark the end of the high-volume tephriphonolitic lava flows from the summit region because no flows of similar morphology are observed spilling over the escarpment.

Petrologic evolution

Previously, Kyle et al. (1992) have discussed the petrologic evolution of Mt. Erebus lavas based on imprecise conventional K/Ar ages. Here, we use the new $^{40}Ar/^{39}Ar$ ages in combination with the geochemical data to evaluate the relationship between apparent age and petrologic evolution.

Geochemical data from Kyle et al. (1992) was used to plot total alkali versus silica (Fig. 6) and Mg number [100(MgO/(MgO+FeO*)] versus $^{40}Ar/^{39}Ar$ apparent age (Fig. 7) for the Mt. Erebus lavas dated in this study. Evident is the progression of Erebus lineage rocks from the oldest, least differentiated lavas (basanite/tephrite) of Cape Barne and Fang Ridge to the youngest, most differentiated lavas (anorthoclase phonolite) of the intracaldera series of modern-Erebus. The petrologic significance of the TAS and Mg# versus age relationships is that

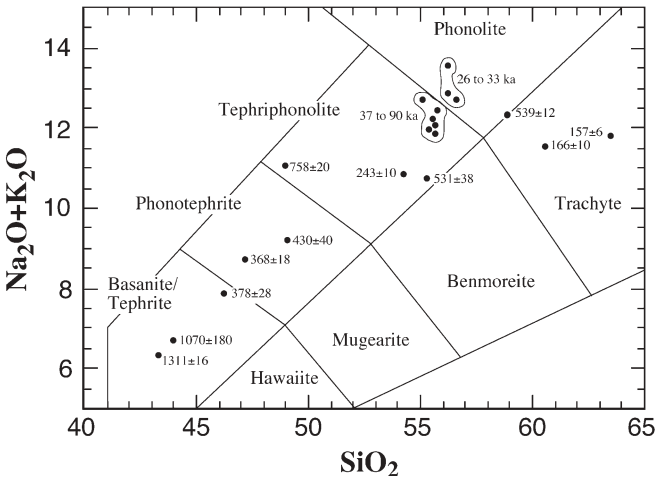

Fig. 6 A total alkali-silica (TAS) diagram, produced with data from Kyle et al. (1992), plotted with Mt. Erebus samples dated in this study (ages in ka). Note that the youngest rocks are among the most differentiated, while the oldest rocks are the least differentiated. Compositional boundaries from Le Bas (1986)

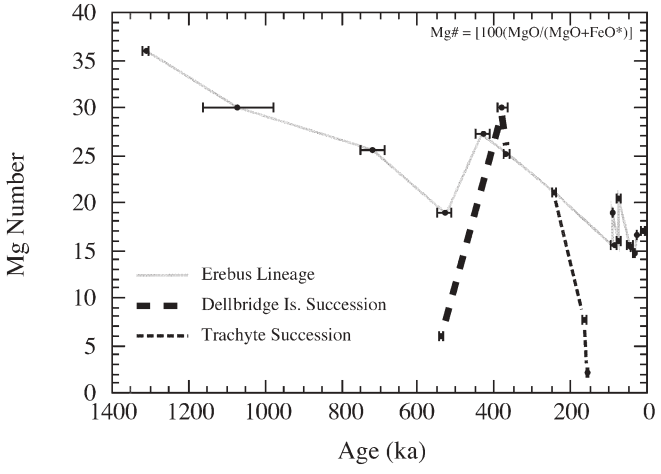

Fig. 7 $^{40}Ar/^{39}Ar$ apparent age plotted versus Mg number [100(MgO/(MgO+FeO*))] (Kyle et al. 1992) where increasing differentiation is represented by decreasing Mg#. A general younging is apparent as differentiation of the Mt. Erebus lavas increase. The Dellbridge Island succession and trachyte succession (characterized by the Aurora Cliffs and Bomb Peak lavas) are noticeably different than that of the Erebus lineage

Mt. Erebus required approximately 1 million years to evolve from a basanite magma system to a phonolitic magma system with very few deviations. Volcanoes of similar geochemical composition have evolved similarly contrasting magma compositions over time spans of only a few hundred thousand years (Anonchea et al. 1990; Panter et al. 1994).

Geochemical deviations are apparent from the Mg# versus $^{40}Ar/^{39}Ar$ apparent age plot, especially around 400–500 ka (Fig. 7). The Abbott Peak tephriphonolite (531±38 ka) has an evolved Mg# of 19 while the phonotephrite SW of Abbott Peak (430±40 ka) has a less evolved Mg# of 27.2, possibly indicating that a large volume of primitive parental basanite was injected into the Erebus magma chamber at about 500 ka.

The Dellbridge Island and Bomb Peak/Aurora Cliffs trachytic successions differ from the straightforward evolution of Erebus lineage lavas from Mt. Erebus (Fig. 7). The Tryggve Point and older (pre 250 ka) Turks Head samples, presumed to be from the Dellbridge Islands succession, are geochemically comparable to Erebus lineage lavas of similar age, but the phonolite from Inaccessible Island is significantly more differentiated than other contemporaneous Erebus lavas. On the Mg# vs. $^{40}Ar/^{39}Ar$ apparent age plot (Fig. 7), an independent array can be assigned to the Dellbridge Island succession indicating that these lavas evolved in a magma chamber separate from that of Mt. Erebus. Likewise, the trachytic lavas of Bomb Peak and Aurora Cliffs form another independent array. The origin of this array is suggestive of assimilation and fractional crystallization (AFC) of a melt of similar composition to that of the tephriphonolite from Turks Head (243±10 ka).

Implications

Several implications of the new $^{40}Ar/^{39}Ar$ apparent age data from Mt. Erebus are apparent. Foremost, these $^{40}Ar/^{39}Ar$ age determinations are significantly younger and more precise than previous K/Ar ages (Treves 1968; Armstrong 1978; Moore and Kyle 1987). The dating of anorthoclase phonolite erratics in Ross Sea drift along the west side of McMurdo Sound (Kyle 1981b) may confirm their derivation from glacially scoured terrains at Capes Barne, Royds and Evans (89–40 ka) thereby better constraining the timing of Ross Sea glaciation. Other fields, such as climatology, may benefit from geochemical/age correlations of Mt. Erebus tephra found within south polar ice cores. Magma generation models of Mt. Erebus can be compared with other similar volcanic regions, possibly improving the understanding of source areas and evolution of alkaline volcanoes.

Eruption rates and volumes

Using the $^{40}Ar/^{39}Ar$ age relationships for Mt. Erebus volcanic rocks and volume estimates, average eruption rates are computed for the proto-Erebus and modern-Erebus volcanoes. These calculations involve several assumptions. Most importantly, the volume of the poorly exposed proto-Erebus volcano is calculated by assuming that the edifice has a symmetrical conical shape. The elevation of Fang Ridge, taken as the height of proto-Erebus, is approximately 3,000 m a.s.l. However, the total volume considers an average depth of 500 m b.s.l. as the starting point for initiation of eruptive activity. Using this model height of the generalized cone of proto-Erebus (~3,500 m), a volume of 1,160 km^3 is calculated. Using a model height of 4,300 m for the entire Mt. Erebus edifice, a volume of 2,170 km^3 is calculated. Subtracting the proto-Erebus

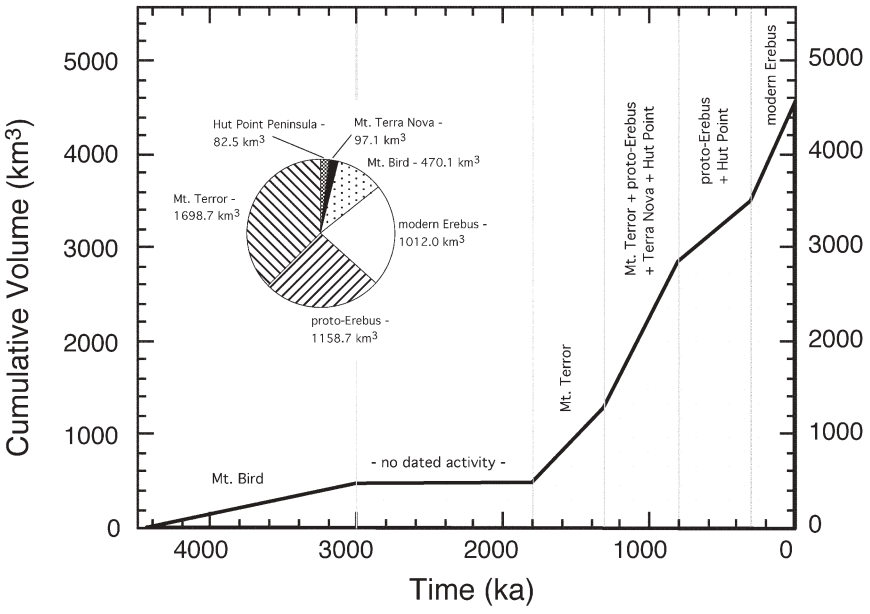

Fig. 8 Cumulative volume curve for Ross Island, Antarctica based on calculated model volumes (see text for procedures), the $^{40}Ar/^{39}Ar$ ages reported in this study and the K/Ar ages of Armstrong (1978)

volume from the whole-Erebus volume results in a modern-Erebus volume of 1,010 km^3. These model volumes also assume that there has not been a significant loss of volume due to explosive eruption or mass wasting. Although Mt. Erebus tephra deposits have been discovered in ice sampled on Mt. Erebus (Harpel et al. 2004) and ~200 km west of Ross Island (Dunbar et al. 1995), their total volume is probably not significant enough to affect eruption rate calculations.

Modeling the timing of volcanic initiation, both for proto-Erebus and for modern-Erebus, requires additional assumptions. The tephritic dike at Cape Barne (~1,300 ka) is assumed to represent the initiation of all eruptive activity at Mt. Erebus. Likewise, the tephriphonolite south of Abbott Peak (342±18 ka) is assumed to represent the cessation of eruptive activity of proto-Erebus. Initiation of modern-Erebus is assumed to have occurred around 250 ka, as suggested by the anorthoclase-phyric tephriphonolite of Turks Head.

Using the model volume data for proto- and modern-Erebus combined with the $^{40}Ar/^{39}Ar$ apparent ages for respective eruptive life spans, calculated average eruption rates for each edifice are distinct. The eruptive rates for proto-Erebus, averaged over its ~950,000-year life span, are approximately 1.2 km^3/1,000 years (km^3/ky). Average eruptive rates for modern-Erebus, over its 250,000-year life span, are approximately 4.0 km^3/ky. The average eruption rate for the entire Mt. Erebus edifice is 1.7 km^3/ky. These differences in eruption rate for Mt. Erebus argue against a steady state output rate over the life of the volcano, as defined for polygenetic volcanoes by Wadge (1982) (i.e. constant rate of magma supply and eruption over a given time period). Although steady state volcanism may have separately occurred for either the proto-Erebus volcano or the modern-Erebus volcano, poor exposure and consequent lack of dates and representative volumes prevent confirmation.

Long-term eruption rates from Mt. Erebus can be compared to the eruption rates of other volcanoes of similar composition. Based on the K/Ar dates from Armstrong (1978) for two other Ross Island volcanoes and generalized model volumes (following the assumptions and procedures used for the Mt. Erebus edifice), Mount Terror, Ross Island has an eruption rate of 1.8 km^3/ky, only slightly higher than that calculated for the entire Mt. Erebus edifice (1.7 km^3/ky). Mount Bird, Ross Island, has a lower eruption rate of 0.3 km^3/ky. Figure 8 shows a cumulative volume curve for the volcanoes of Ross Island and their respective eruption rates. Mt. Etna, Italy, is a subduction-related volcano of similar size and composition, yielding a higher steady state eruption rate of 8.2 km^3/ky (Wadge 1980). Tenerife Island, in the Canary Islands, is an oceanic-island alkaline volcano with an eruption rate for the subaerial portions of the island of 0.2 to 1.8 km^3/ky (Ancochea et al. 1990). Other intraplate volcanoes have eruption rates which are significantly higher than those calculated for Mt. Erebus (e.g. Mauna Loa at 20.8 km^3/ky; Wadge 1980). The only two intracontinental volcanoes with available data are based on relatively short-term eruption records (<200 years), extrapolated here to 1,000 years. The calculated eruption rates for Vesuvius (Italy) and Nyamuragira (Africa) are 9.2 and 12.0 km^3/ky, respectively (Wadge 1980). These data indicate that, although Mt. Erebus grew at an accelerated rate beginning about 250 ka with eruptions of anorthoclase-phyric tephriphonolite lavas, its eruption rates are significantly lower than those of other volcanoes of similar geochemical composition.

Implications for the calculated eruption rates of Mt. Erebus include the calculation of plume rise rate. Using a simplified equation, Kyle et al. (1992) derived a plume rise rate for Mt. Erebus of approximately 65 mm/year. This rise rate however was determined using conventional K/Ar ages of approximately 1 million years (Armstrong

1978). Using the same methods employed by Kyle et al. (1992) with the new $^{40}Ar/^{39}Ar$ apparent ages of this study, a mantle rise rate can be determined for both proto- and modern-Erebus.

Kyle et al. (1992) used values for the fractionation of basanite required to produce phonolite (25% residual liquid) or phonotephrite (45% residual liquid) based on the presumed volumes of those respective magma types on Mt. Erebus. These values were then used to calculate the volume of basanite and mantle material necessary to yield the volumes of lava presently observed at Mt. Erebus. Based on the above values, the calculated volumes of parental basanite required to account for the model volumes of proto- and modern-Erebus are 1,270 and 3,238 km^3, respectively. Assuming basanite is derived from garnet lherzolite, a 5% degree of partial melt of 25,402 and 64,768 km^3 of mantle is required to produce the parental basanite of proto- and modern-Erebus, respectively. Kyle et al. (1992) assumed a plume diameter of 40 km. If the same diameter were used here, cylinders of length 20.2 km (proto-Erebus) and 36.8 km (modern-Erebus) would be necessary to accommodate the volumes of mantle calculated above. Using the same eruptive life spans used to calculate eruption rates, plume rise rates for proto-Erebus would be 21.2 mm/year, and modern-Erebus would be 147.3 mm/year. These high source rise rates, especially for the modern-Erebus lavas (<250 ka), support the conclusion of Kyle et al. (1992) that a large volume of mantle plume material is necessary to supply the basanite which differentiated to form the lavas on Mt. Erebus.

Conclusions

$^{40}Ar/^{39}Ar$ ages from anorthoclase separates are an order of magnitude younger and more precise than published conventional K/Ar dates from Mt. Erebus. This is largely due to the removal of excess-argon-bearing melt inclusions by rigorous sample preparation.

Together with the larger number of samples dated, the increase in analytical precision and accuracy provides a more comprehensive history of the Mt. Erebus edifice. Beginning with the building of a broad, mafic shield volcano at about 1,300 ka, the edifice termed proto-Erebus continued to erupt tephrites, basanites and phonotephrites until approximately 350 ka. After 718 ka, a catastrophic event near the summit resulted in a remnant escarpment (Fang Ridge). By ~250 ka, activity apparently shifted a few kilometers to the southwest and became more differentiated. This was the beginning of modern-Erebus activity, characterized by anorthoclase-phyric tephriphonolite and phonolite. Average eruption rates for pre- and post-250 ka Erebus are estimated at 1.2 km^3/ky and 4.0 km^3/ky, respectively. These cone-building rates for the two Mt. Erebus edifices are smaller than volcanoes of similar geochemistry and tectonic setting.

Acknowledgements This work was supported by grants from the Office of Polar Programs, National Science Foundation. Additional funding came from within the NMGRL at the New Mexico Bureau of Geology and Mineral Resources. The authors would like to thank Nelia Dunbar for her discussions on magma chemistry and melt inclusion properties. Additional thanks goes to NSF, the Antarctic Support Associates and the US Navy VXE-6 squadron who provided the necessary field support. Improvements in the manuscript resulted from reviews by J. Kelly Russell and Andrew Calvert.

References

Ancochea E, Fuster JM, Ibarrola E, Cendrero A, Coello J, Hernan F, Cantagrel JM, Jamond C (1990) Volcanic evolution of the island of Tenerife (Canary Islands) in the light of new K-Ar data. J Volcanol Geotherm Res 44:231–249

Armstrong RL (1978) K-Ar dating: Late Cenozoic McMurdo Volcanic Group and Dry Valley glacial history, Victoria Land, Antarctica. NZ J Geol Geophys 21:685–698

Cande SC, Kent DV (1992) A new geomagnetic polarity time scale for the Late Cretaceous and Cenozoic. J Geophys Res 97:13917–13951

Chester DK, Duncan AM, Guest JE, Kilburn CRJ (1985) Mount Etna, the anatomy of a volcano. Chapman and Hall, London, pp 1–404

Cooper AK, Davey FJ, Behrendt JC (1987) Seismic stratigraphy and structure of the Victoria Land basin, western Ross Sea, Antarctica. In: Cooper AK, Davey FJ (eds) The Antarctic Continental Margin: geology and geophysics of the western Ross Sea. Circum-Pacific Council for Energy and Resources, Houston, pp 27–65

Deino A, Potts R (1990) Single-crystal $^{40}Ar/^{39}Ar$ dating of the Olorgesailie Formation, Southern Kenya Rift. J Geophys Res 95:8453–8470

Dunbar NW, Kyle PR, McIntosh WC, Esser RP (1995) Tephra layers in blue ice, Allan Hills, Antarctica: a new source of glacial tephrochronological data. In: IUGG XXI General Assembly, Abstracts, p A303

Esser RP, Kyle PR, McIntosh WC (2003) Data Repository for "$^{40}Ar/^{39}Ar$ dating of the eruptive history of Mount Erebus, Antarctica: volcano evolution." New Mexico Bureau of Geology and Mineral Resources Open File Report OF-AR-20

Esser RP, McIntosh WC, Heizler MT, Kyle PR (1997) Excess argon in melt inclusions in zero-age anorthoclase feldspar from Mt. Erebus, Antarctica, as revealed by the $^{40}Ar/^{39}Ar$ method. Geochim Cosmochim Acta 61:3789–3801

Foland KA, Fleming TH, Heimann A, Elliot DH (1993) Potassium-argon dating of fine-grained basalts with massive Ar loss: application of the $^{40}Ar/^{39}Ar$ technique to plagioclase and glass from the Kirkpatrick Basalt. Antarctica Chem Geol 107:173–190

Funaki M (1983) Paleomagnetic investigation of McMurdo volcanics, Antarctica. Nankyoku Shiryo 77:1–19

Guest JE, Duncan AM, Chester DK (1988) Monte Vulture Volcano (Basilicata, Italy): an analysis of morphology and volcaniclastic facies. Bull Volcanol 50:244–257

Harpel CJ, Kyle PR, Caldwell, DA, McIntosh WC, Esser RP (2004) ^{40}Ar /^{39}Ar dating of the eruptive history of Mount Erebus, Antarctica: summit flows and caldera collapse. Bull Volcanol (in review)

Kyle PR (1976) Geology, mineralogy, and geochemistry of the Late Cenozoic McMurdo Volcanic Group, Victoria Land, Antarctica. Unpublished PhD Thesis, Victoria University, Wellington

Kyle PR (1977) Mineralogy and glass chemistry of recent volcanic ejecta from Mt. Erebus, Ross Island, Antarctica. NZ J Geol Geophys 20:1123–1146

Kyle PR (1981a) Mineralogy and geochemistry of a basanite to phonolite sequence at Hut Point Peninsula, Antarctica, based on core from Dry Valley Drilling Project Drillholes 1, 2 and 3. J Petrol 22:451–500

Kyle PR (1981b) Glacial history of the McMurdo Sound area as indicated by the distribution and nature of McMurdo Volcanic Group rocks. In: McGinnis LD (ed) Dry Valley Drilling Project. AGU, Washington, DC

Kyle PR (1990a) McMurdo Volcanic Group-Western Ross Embayment: introduction. In: LeMasurier W, Thomson J (eds) Volcanoes of the Antarctic Plate and Southern Oceans. Antarctic Research Series. Am Geophys Union, Washington, DC, pp 18–25

Kyle PR (1990b) Erebus Volcanic Province: Summary. In: LaMasurier W, Thomson J (eds) Volcanoes of the Antarctic Plate and Southern Oceans. Antarctic Research Series. Am Geophys Union, Washington DC, pp 81–88

Kyle PR (1990c) Melbourne volcanic province; Summary: In: LaMasurier W, Thomson J (eds) Volcanoes of the Antarctic Plate and Southern Oceans. Antarctic Research Series. Am Geophys Union, Washington DC, pp 48–52

Kyle PR (1994) Volcanological and environmental studies of Mount Erebus, Antarctica. In: Antarctic Research Series. AGU, Washington DC, p 162

Kyle PR, Cole JW (1974) Structural control of volcanism in the McMurdo Volcanic Group, Antarctica. Bull Volcanol 38:16–25

Kyle PR, Dibble RR, Giggenbach WF, Keys HJ (1982) Volcanic activity associated with the anorthoclase phonolite lava lake, Mount Erebus, Antarctica. In: Craddock C (ed) Antarctic geoscience. The University of Wisconsin Press, Madison, Wisconsin, p 1172

Kyle PR, Moore JA, Thirlwall MF (1992) Petrologic evolution of anorthoclase phonolite lavas at Mount Erebus, Ross Island, Antarctica. J Petrol 33:849–875

Le Bas MJ, Le Maitre RW, Streckeisen A, Zanetti B (1986) A chemical classification of volcanic rocks based on the total alkali silica diagram. J Petrol 27:745–750

Lo CH, Onstott TC, Chen CH, Lee T (1994) An assessment of $^{40}Ar/^{39}Ar$ dating for the whole rock volcanic samples from the Luzon Arc near Taiwan. Chem Geol 114:157–178

Macdonald GA (1965) Hawaiian calderas. Pacific science 19:320–334

Mankinen EA, Cox A (1988) Paleomagnetic investigation of some volcanic rocks from the McMurdo Volcanic Province, Antarctica. J Geophys Res 93:1599–11612

Moore JA (1986) Mineralogy, geochemistry and petrogenesis of the lavas of Mount Erebus, Antarctica. Unpublished Master's Thesis, New Mexico Institute of Mining and Technology

Moore JA, Kyle PR (1987) Volcanic geology of Mount Erebus, Ross Island, Antarctica. In: NIPR Symposium on Antarctic Geosciences. National Institute of Polar Research, Tokyo, pp 48–65

Panter KS, McIntosh WC, Smellie JL (1994) Volcanic history of Mount Sidley, a major alkaline volcano in Marie Byrd Land, Antarctica. Bull Volcanol 56:361–376

Siebert L (1984) Large volcanic debris avalanches: characteristics of source areas, deposits, and associated eruptions. J Volcanol Geothermal Res 22:163–197

Singer BS, Pringle MS (1996) Age and duration of the Matuyama-Brunhes geomagnetic polarity reversal from $^{40}Ar/^{39}Ar$ incremental heating analyses of lavas. Earth Planet Sci Lett 139:47–61

Steiger RH, Jager E (1977) Subcommission on geochronology: convention on the use of decay constants in geo- and cosmochronology. Earth Planet Sci Lett 36:359–362

Taylor JR (1982) An introduction to error analysis: the study of uncertainties in physical measurements. Univ Sci Books, Mill Valley, Calif., p 270

Treves SB (1968) Volcanic rocks of the Ross Island area. Antarctica J US 3:108–109

van den Bogaard P (1995) $^{40}Ar/^{39}Ar$ ages of sanidine phenocrysts from Laacher See Tephra (12900 yr B.P.): chronostratigraphic and petrologic significance. Earth Planet Sci Lett 133:163–174

Wadge G (1980) Output rate of magma from active central volcanoes. Nature 288:253–255

Wadge G (1982) Steady state volcanism; evidence from eruption histories of polygenetic volcanoes. JGR J Geophys Res B 87:4035–4049

Walker GPL (1988) Three Hawaiian calderas: an origin through loading by shallow intrusions? J Geophys Res 93:14773–14784